Annals of Nuclear Energy 98 (2016) 12–18

Contents lists available at ScienceDirect

Annals of Nuclear Energy

journal homepage: www.elsevier.com/locate/anucene

Thermal-hydraulic analysis of an integrated spallation target module in ADS

He Mei-sheng, Bai Yun-qing *, Zhang Yong, Song Yong, Zhao Zhu-min

Key Laboratory of Neutronics and Radiation Safety, Institute of Nuclear Energy Safety Technology, Chinese Academy of Sciences, Hefei, Anhui 230031, China

ARTICLE INFO

Article history:
Received 1 December 2015
Received in revised form 29 June 2016
Accepted 6 July 2016

Keywords:
ADS
Integrated spallation target
Thermal-hydraulics analysis
Geometry modification

ABSTRACT

As a key component in Accelerator Driven System (ADS), the spallation target is exposed to high irradiation intensity radiation, and a larger amount of heat is deposited on it. Therefore, the cooling of the target is a challenging task in the target design. Integrated target module with a solid beam window, and cooled by reactor primary coolant is a good contender for ADS system. The numerical analysis of two target modules was performed by using finite element code to assess the target cooling capacity. It was found that with uniform inlet velocity, the geometry modification of the inlet could improve the heat transfer effectively. But with non-uniform inlet velocity, the geometry modification of the inlet had little effect on cooling capacity.

© 2016 Elsevier Ltd. All rights reserved.

1. Introduction

In Accelerator Driven System (ADS), a high-energy proton beam impinges on target materials to produce spallation neutrons, and these neutrons are multiplied by subcritical core to transmute long-lived fission products (LLFP) or miner actinide (MA) (Nifenecker et al., 2003). The ADS is being considered as a promising solution to transmute long-lived nuclear wastes (Cho et al., 2008). In most nuclear power stations, lager program associated with ADS R&D is been actively pursued: XADS (Cinotti and Gherardi, 2002) and MYRRHA (Abderrahim et al., 2012) in the European commission, ATW (DOE, 1999) in the USA, OMEGA (Mukaiyama et al., 2001) in Japan, and HYPER (Park et al., 2000) in Korean.

Chinese Academy of Sciences (CAS) is conducting research and development (R&D) on the Accelerator Driven System (ADS) (Zhan and Xu, 2012; Wu, 2016a). Based on years of the research in the field of advanced neutronics software (Wu et al., 2015), low radioactivity material (Huang et al., 2014), and advanced nuclear system design (Qiu et al., 2000; Wu et al., 2011), Institute of Nuclear Energy Safety Technology (INEST), CAS undertakes the R&D of the lead-bismuth eutectic (LBE) cooled reactor design and technology (Wu, 2016b; Wu et al., 2016c).

In previous studies, many projects put forward their target design, like JAEA-ADS (Kikuchi, 2009), HYPER (Song and Tak, 2003), FASTEF (Abderrahim et al., 2012), THREE BEAM CONCEPT (Knebel et al., 2000), XADS (Coors et al., 2004) and MYRRHA (Class et al., 2011). In these contributions, LBE is today the reference target material for ADS application (OECD, 2005; Bauer, 2010). And the target unit with a solid beam window cooled by reactor primary coolant, has the stable target material surface and the radioactivity production containment. It will simplify a target system that increase the neutron economy and reduce the investment cost. And there have been intensive studies on the material (Alamo, 2003), thermal hydraulics, configuration and safety analysis (Song and Tak, 2003; Coors et al., 2004; Saito et al., 2006; Tak et al., 2005).

A proton beam enters the target unit from the top, penetrates the beam window and impinges on the upward flowing LBE. In spallation region, about 60–70% of the beam power is deposited as heat in the target materials (Cho et al., 2008; Cinotti et al., 2003). It is necessary to demonstrate that the target would be cooled adequately. The beam window is a thin barrier to separate the vacuum space from the liquid LBE. Exposed to the proton beam, the window undergoes a high temperature and irradiation. From the thermal-hydraulic point of view, the main issue of the window target is the cooling capability of the window.

In this paper, the Newton's law of cooling and the Fourier law is applied to evaluate the temperature on the window. And this paper presents the numerical studies on the target systems. Two target schemes with different geometry configurations are compared by using a commercial code CFX (ANSYS Inc., 2011).

2. Description of target system

Several design concepts have been developed for the target system. One of the typical designs (Cho et al., 2008) is shown in Fig. 1.

* Corresponding author.
E-mail address: yunqing.bai@fds.org.cn (Y.-q. Bai).

http://dx.doi.org/10.1016/j.anucene.2016.07.005
0306-4549/© 2016 Elsevier Ltd. All rights reserved.

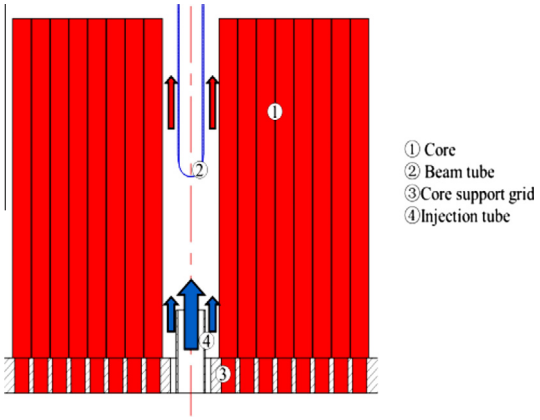

Fig. 1. Schematic view of the typical target design.

In contrast to the proposed target, the target channel surrounded by assemblies which is nearly cylinder. The target channel diameter is set at 260 mm. LBE at about 300 °C driven by the main primary pump from the flow distribution, rises in the space between the sleeve and the beam tube to remove the deposited heat. Then, the hot LBE is pumped from the hot pool, through the main heat exchange and down over pump to complete the LBE circuit. An injection tube is placed at the inlet of the target channel and divides the inlet into two zones. The velocity in the central zones is larger than that of the outer zones. The injection tube diameter and thickness are 168 mm and 10 mm, respectively. In the channel, the beam tube with a hemi-spherical window is adopted for the target. A thickness of the window about 2 mm is chosen in this scheme, and the inner diameter is about 150 mm.

Schematic view of the proposed integrated target unit is shown in Fig. 2. It is demonstrated that the target is horizontally located in the center of the reactor core, and vertically hung on the reactor cover at the top. In general, the target module consists of a cylindrical steel sleeve from outside and a co-axis cylindrical beam tube with a suitable spacing for LBE flowing. The beam tube closed by a hemi-spherical window is adopted for the target.

A uniform proton beam with radius of 50 mm is selected to perform the spallation process. Assuming the proton beam with 250 MeV power and 5 mA intensity penetrates the beam window, deposited energy as heat in spallation region is about 1.2 MW. As shown in Fig. 3, the coolant flows into the gap between the beam tube and the sleeve, and removes the deposited heat. And then, it runs out at the orifices on the sleeve side wall and mixed with the reactor coolant in the hot pool. The vertical section of the spallation area is inverted cone sharp. It allows minimizing the inactive volume of LBE in the target flow channel and increasing the window surface heat transfer.

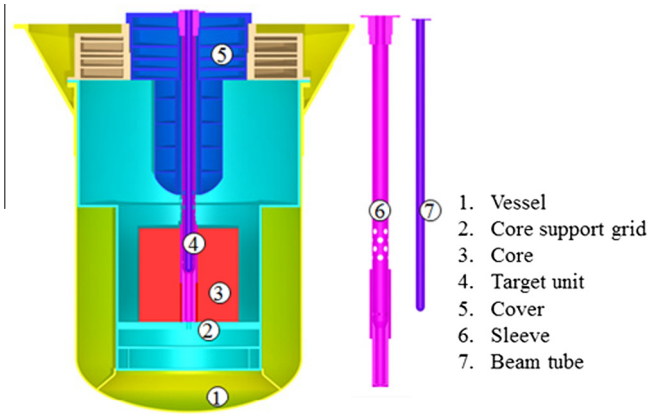

Fig. 2. Overall views of the integrated target design.

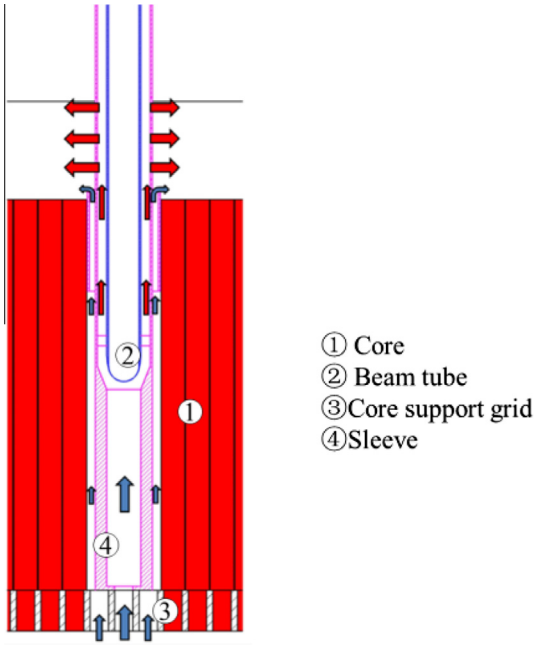

Fig. 3. Thermal hydraulic schematic view of the integrated target.

The modified 9Cr1Mo ferritic–martensitic steel (T91) is the reference window material for the present study (Tak et al., 2005). And other structure parts are made of stainless steel 316 L.

3. Theoretical methodology

The temperature of the target window can be analyzed by the Newton's law of cooling and the Fourier law. The structure of the window can be seen in the Fig. 4. r_1, r_2 is the radius of the inner and outer window surface.

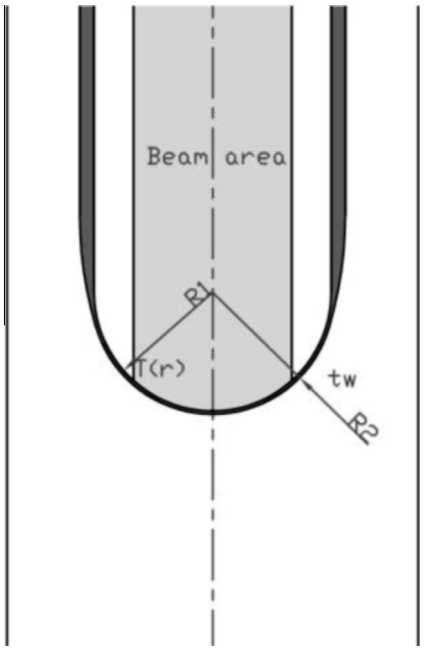

Fig. 4. The structure of the target window.

3.1. Heat transfer between fluid and window surface

To express the overall effect of convection, we use Newton's law of cooling:

$$\emptyset = hA(t_w - t_f) \tag{1}$$

where, $\emptyset$ is the total power of the heat that deposited in the window, h is called the convection heat-transfer coefficient, A is the area of the region passed by the proton beam in the wet window surface, t_w and t_f is the temperature of the window wet surface and LBE bulk. Here the heat transfer rate is related to the overall temperature difference between the window and coolant and the surface area A.

For the constant heat flux case, the convection heat transfer coefficient is given by

$$h = \frac{N_u \lambda_{LBE}}{l} \tag{2}$$

where, N_u is the Nusslet number that represents the intensity of convective heat transfer, l is the characteristic length, and λ_{LBE} is the thermal conductivity of the stationary LBE.

From the experiment results, Nusselt number can be described by the following equation (Tsujimoto et al., 2007):

$$N_u = 0.6852 P_e^{0.6626} \tag{3}$$

where, P_e is the Peclet number relevant in the study of transport phenomena in a continuum.

Before arrived at window, the fluid is heated by the heat deposited in the coolant bulk. The equation that relates the heat with temperature is:

$$q = C_p \rho v A_{channel} (t_f - t_{inlet}) \tag{4}$$

where, q is the power of the heat deposited in the LBE bulk, v is the average coolant velocity, $A_{channel}$ is the area of the flow channel, and t_{inlet} is the temperature of the coolant inlet.

3.2. Heat conduction through the window

The heat conduction in the window can be described by the Fourier law:

$$q = -k\frac{\partial T}{\partial n} = -k\nabla T \tag{5}$$

where, q is the heat flux, k is the thermal conductivity of the window material.

For steady state heat conduction, Eq. (5) can be simplified into the following form:

$$\nabla^2 T + \frac{q_v}{k} = 0 \tag{6}$$

Assuming the volumetric heat release rate is constant, the Eq. (6) can be converted to one dimensional problem. The boundary conditions of the Eq. (6) is:

$$r = r_1, \ \frac{dT}{dr} = 0 \tag{7}$$

$$r = r_2, \ T = t_w \tag{8}$$

The functional relationship of the temperature along the window thickness is:

$$T(r) = t_w + \frac{q_v}{6k}(r^2 - r_1^2) + \frac{q_v r_1^3}{3k}\left(\frac{1}{r} - \frac{1}{r_1}\right) \tag{9}$$

4. Thermal-hydraulic analysis model

It is assumed that the target works under normal, steady-state operating conditions. The proton beam is at full power, and the pumps are functioning normally. Thermal-hydraulics simulations are being undertaken to compare the cooling capability of the typical target and the integrated target. In addition, due to the LBE corrosion and radiation damage, the design criteria were set: (1) the flow velocity of LBE should not exceed 2 m/s; (2) the temperature of the structure material should not exceed 550 °C.

4.1. Computational model

The CFD model of the two target schemes is shown in Fig. 5. The model used in this study consists of the LBE fluid and the beam tube. The fluid domain only includes the LBE which flows through the spallation region. The region of the fluid is from the core support plate to the LBE free surface. The beam tube located in the center of the LBE fluid is the solid domain. The interfaces between the solid and fluid domain can transfer heat flux.

The grid considered for the spallation region is depicted in Fig. 6. The typical design used in this study consists of 528,171

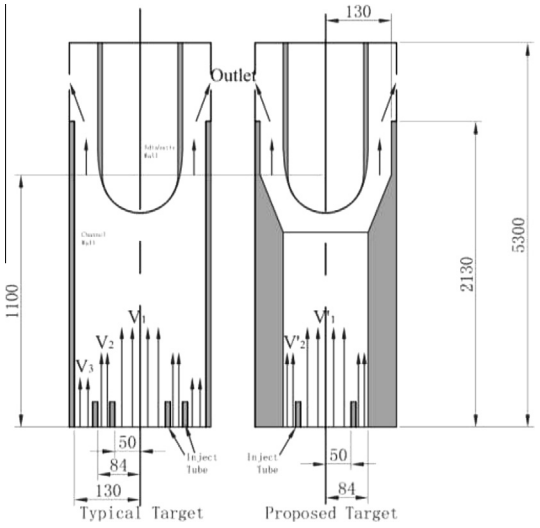

Fig. 5. Computational domain and boundary conditions.

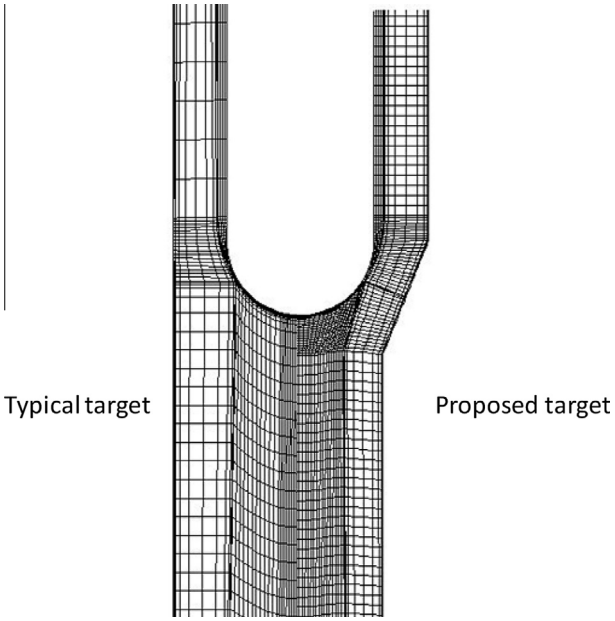

Fig. 6. Computational meshes of the two targets.

fluid cells and 87,126 structure elements. Proposed design (proposed design) consists of 471,340 fluid cells and 101,256 structure elements. In the vertical direction, a fine mesh is employed near the walls and a coarse mesh in the center, in order to achieve appropriate y+ value (in the range 30–100). Fig. 7 shows the y+ distribution along the outer surface of the window. The main data used in the calculation is listed in Table 1.

4.2. Boundary conditions

As previously mentioned, the proton beam has a uniform radial distribution on the beam window. The deposited heat in the both LBE and target window is calculated by using Monte Carlo method software, FLUKA. The power deposition profile in the LBE target material and beam window is shown in Fig. 8. In FLUKA calculation, fine meshes were adopted near window to satisfy the CFD requirements. The grid size is 0.2 mm. Fig. 9 shows the heat deposition in the window. The heat deposition density in the window is about 0.34 kW/(m^3 mA) in the beam region and out the beam region it is almost zero. Fig. 10 shows the heat deposition in LBE bulk. Due to the Bragg peak, the maximum heat deposition density, 0.6 kW/(m^3 mA), is located around 7 cm below the window. The 3D deposited heat data is imported to CFX with CEL.

As shown in Fig. 5, the inlet of typical design is divided into three zones. The inlet velocities from inside to outside are v_1, v_2, v_3, respectively. The predicted inlet velocities of proposed design are v_1', v_2'. The inlet temperature of two models is 300 °C. The thermal-hydraulic analysis considered uniform and non-uniform inlet velocity schemes and geometrical variations. The main inlet parameters considered are summarized in the Table 2. The flow of LBE is upwards in the fluid domain over the window and flows out the sidewall. The outlet in the side is a constant-pressure outlet. The Reynolds number at the inlet is 3.3×10^6, so the flow is turbulent. To take account of the turbulence effects, the sheer stress transport (SST) model has been employed. The auto timescale control is used in this simulation and the timescale factor is 0.5.

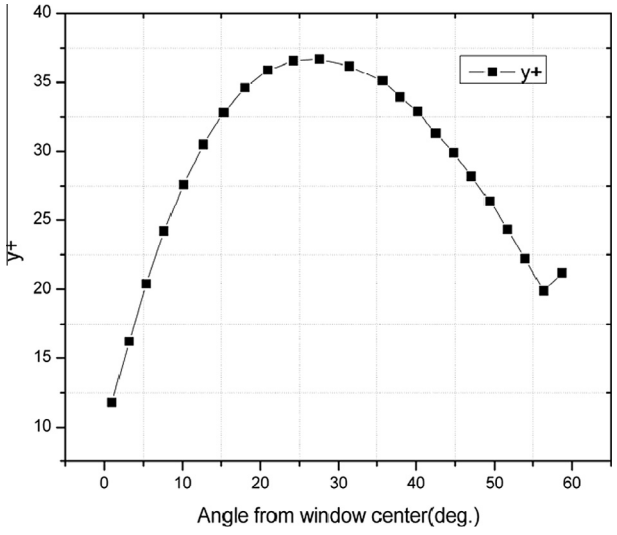

Fig. 7. y+ profile along the outer surface of the window.

Table 1
Main data used for the calculation.

Boundary conditions	LBE inlet temperature	300 °C
	Other wall	Adiabatic
Material characteristics of LBE	Density	10,390 (kg/m^3)
	Thermal conductivity	11.2 (W m^{-1} K^{-1})
	Heat capacity	146.5 (J kg^{-1} K^{-1})
	Viscosity	0.0020332 (Pa s^{-1})
Material characteristics of T91	Thermal conductivity	25.2 (W m^{-1} K^{-1})
Solution	Turbulence model	SST

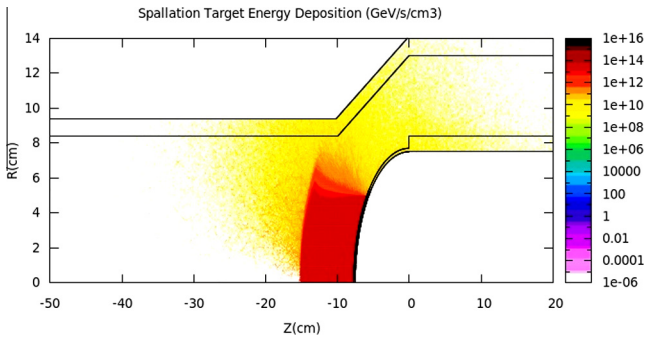

Fig. 8. The deposited heat distribution in target.

4.3. Validation

4.3.1. Influence of grid size

The prediction of turbulent quantities is usually quite sensitive to the number of grid nodes used in the interface and solution

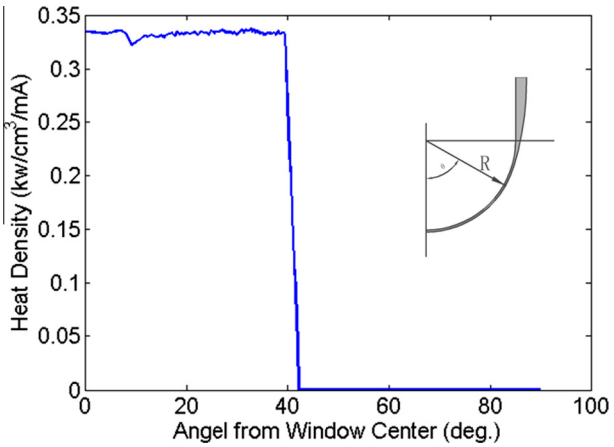

Fig. 9. Heat deposition distribution in the window.

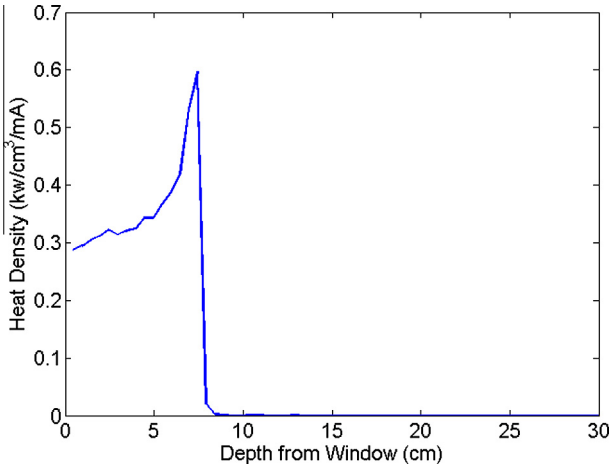

Fig. 10. Heat deposition distribution in the LBE.

Table 2
The inlet parameters considered in the thermal-hydraulic analysis.

Model	Mass flow rate	Inlet velocity	Inlet temperature
Typical target	193.33 kg/s	$v_1 = v_2 = v_3 = 0.35$ m/s	300 °C
Proposed target	193.33 kg/s	$v'_1 = v'_2 = 0.85$ m/s	300 °C
Typical target	193.33 kg/s	$v_1 = 1.8$ m/s; $v_2 = 0.3$ m/s; $v_3 = 0.01$ m/s	300 °C
Proposed target	193.33 kg/s	$v'_1 = 1.95$ m/s; $v'_2 = 0.23$ m/s	300 °C
Proposed target	166.56 kg/s	$v'_1 = 1.95$ m/s; $v'_2 = 0.05$ m/s	300 °C

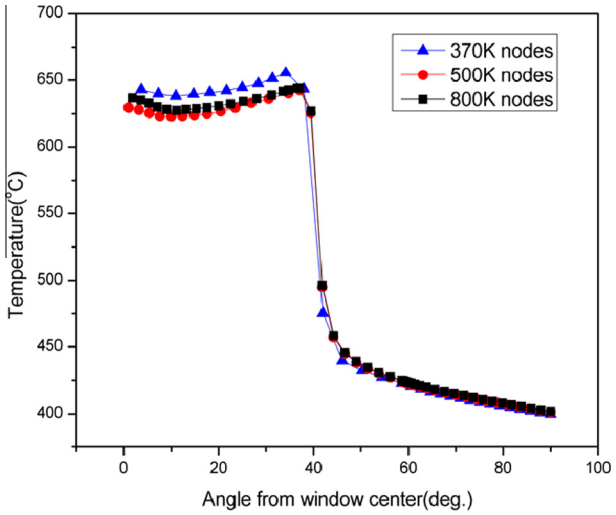

Fig. 11. Influence of grid size of predicted results.

domain. Thus it is very important to use an adequate number of computational cells while numerically predicted contour plots and profiles of solid hold solving the governing equations over the solution domain. For proposed design, in the present work, three grid sizes were considered to study the effect of grid size on prediction of temperature distribution. The chart of the temperature distribution along the window is show in Fig. 11. It can be seen that the influence of the grid size within the considered range was very small.

4.3.2. Heat transfer

The validation of CFD codes is still not completed in specific areas such as turbulent heat transfer in liquid metals. In present work, the benchmark of the CFD code of the heat transfer is presented for the proposed target.

The deposited heat in coolant bulk is neglect. With the beam current 5 mA, the heat deposition in the window is 30.5 kW. The inlet velocities from inside to outside are 1.95 m/s, 0.05 m/s, respectively. The inlet temperature is set as 300 °C.

In simulation, the average temperature of the wet window surface in the beam region is about 384 °C. And the average velocity near the window in beam region is around 0.8 m/s. According to theoretical formula, the temperature is 390.074 °C. In this calculation, the characteristic length is set as 0.09 m. The relative errors of the numerical results and the theoretical correction are within the range of 7%.

5. Results and discussion

5.1. Uniform inlet velocity

At first, the inlet in the divided zone is the same. In typical design, v_1 equals v_2 and v_3. And in proposed design, v'_1 equals v'_2. Both of the models have same mass flow rate, 193.33 kg/s.

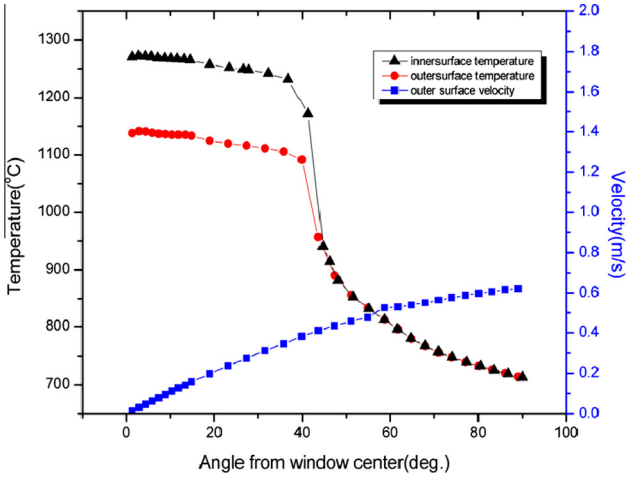

Fig. 12. The temperature and the velocity for the typical target window with uniform inlet velocity.

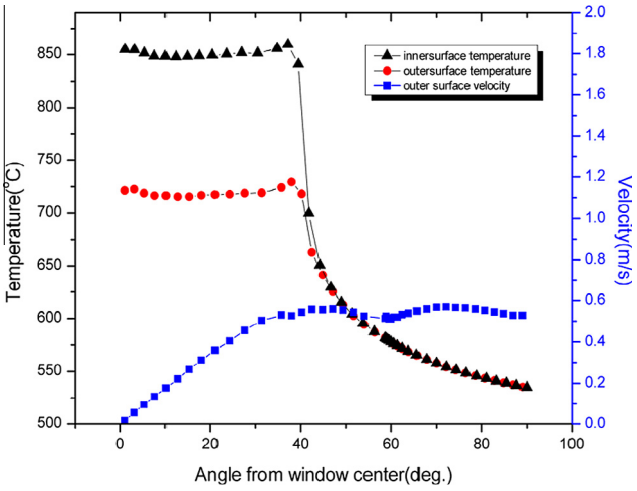

Fig. 13. The temperature and the velocity for the proposed target window with uniform inlet velocity.

Fig. 12 shows the temperature and the velocity along the window surface of the typical target. As expected, flow stagnation near the center of the window can be clearly seen. In this area, it is difficult to improve the heat transfer of the beam window. The maximum temperature occurs in the center of the inner surface, and is as high as 1255.5 °C, which is well above the required temperature limits of the structural material. In the beam region, the temperature drops gradually. A massive decrease of temperature is appeared at approximately 40° from the window center. The maximum temperature drop across the window thickness is about 132 °C. According to the Eq. (9), the temperature drop across the window is 132.584 °C. The relative error of the numerical results and theoretical correction formula is within the range of 0.5%.

Fig. 13 shows the temperature and the velocity distribution along the window surface of the proposed target. The trend of the temperature change of the proposed target is similar to the typical target. By the modification of the channel form, the maximum temperature falls off to 846 °C. But this temperature is still above the temperature limit. The maximum temperature drop across the window thickness is 132 °C.

Comparing the peak temperature, obviously, the proposed design can rapidly reduce the maxim temperature in the window. This is due to the increasing velocity near the beam window that

enhanced the heat transfer between the window and the coolant bulk. The result is performed as expected.

5.2. Non-uniform inlet velocity

From the uniform results, the velocity near the window is an important design parameter affecting the heat transfer. Referring to the HYPER design, the typical design inlet is divided into three zones. The inlet velocities (v_1, v_2 and v_3) are 1.8, 0.3, 0.01 m/s, respectively.

Fig. 14 shows the temperature and the velocity distribution of the typical target. The maximum velocity is 1.834 m/s, and is less than the material limit (2 m/s). Relatively faster LBE stream is formed in the central region by the strong innermost injection. The maximum temperature occurs near the beam boundary of the inner window surface, and is 651.3 °C, which is just above the required temperature limits of the structural material. The maximum temperature drop across the window thickness is 132.8 °C.

With the same mass flow rate, the inner inject velocity v_1' of the proposed target is 1.95 m/s, and the outer inject v_2' is 0.23 m/s. Fig. 15 shows the results with the proposed target. The maximum temperature is 668.3 °C and is above the typical target. The maximum temperature drop across the window thickness is 132 °C.

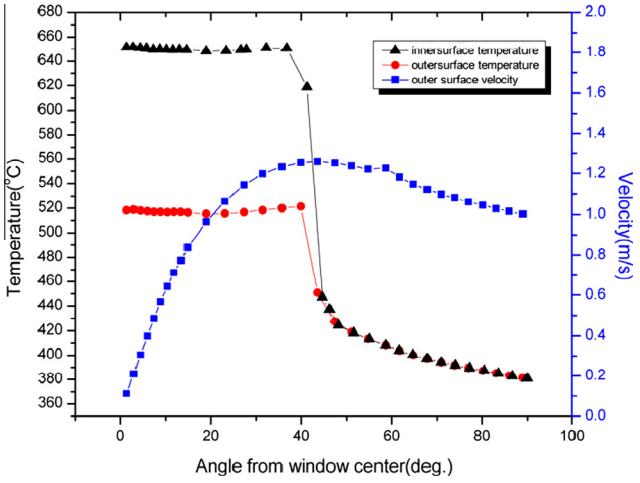

Fig. 14. The temperature and the velocity for the typical target window with non-uniform inlet velocity.

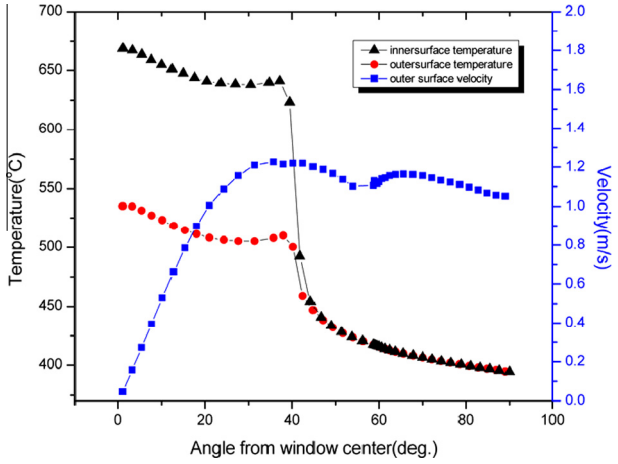

Fig. 15. The temperature and the velocity for the proposed target window non-uniform inlet velocity (1.95 m/s, 0.23 m/s).

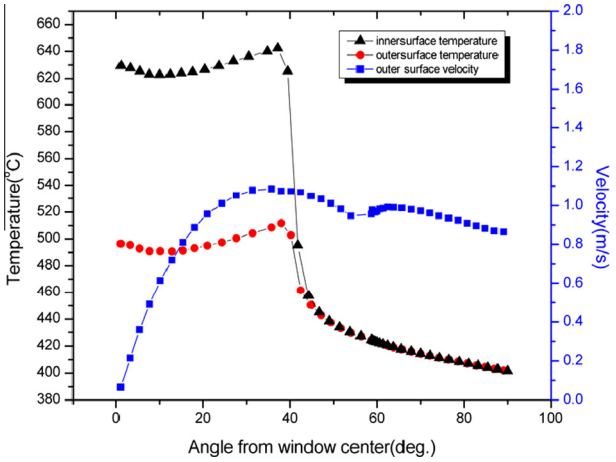

Fig. 16. The temperature and the velocity for the proposed target window non-uniform inlet velocity (1.95 m/s, 0.05 m/s).

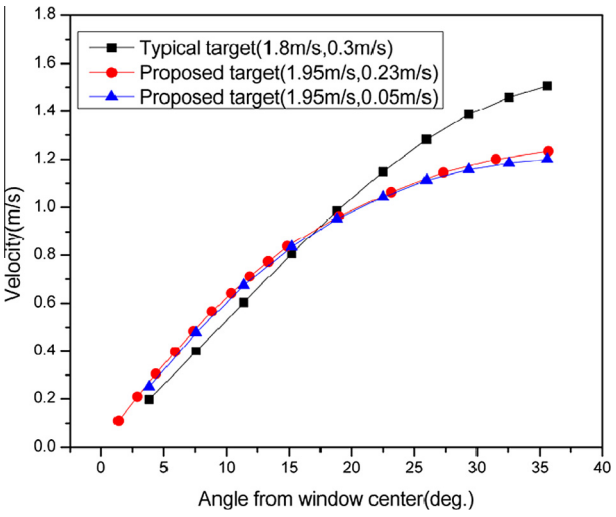

Fig. 17. The velocity distribution on the window of different target models.

To increase the velocity near the center of the window, the outer inject velocity dropped to 0.05 m/s. In this case, the result of the temperature and the velocity on the window are shown in the Fig. 16. The maximum temperature is reduced by 42.9 °C and lower than the typical design. The maximum temperature drop across the window thickness is 132.1 °C.

From the heat transfer equations we discussed above, the velocity on the beam region of the target wet surface and the coolant temperature is the main effect of the window temperature. The velocity results of three cases are show in Fig. 17. The average velocity of three cases is nearly same. The velocity with 1.95 m/s and 0.23 m/s of the proposed target in the center of the window is lower than the others. So the heat in this area of the window is difficult to remove. The velocity distribution of the other cases is nearly same. So these cases have similar temperature. The temperature drop across the window in all calculations is the same, that is consistent with the theoretical calculation.

6. Conclusion

Due to the intense heat deposition and the limited space in the reactor core, the target geometrical configuration and the inlet flow distribution had been carefully designed to ensure adequate

coolant velocity for cooling the target material. CFD analyses were performed to define the velocity and the temperature distribution in the window and the coolant bulk. The results achieved are summarized as follows:

In the uniform inlet condition, the maximum temperature on the window of the typical design is 1255.5 °C. With same mass flow rate, the maximum temperature on the window of the proposed design is reduced to 846 °C. While an increase in the inlet velocity to about 3 times, the temperature difference has reduced by 40%.

The inlet flow velocity is an important design parameter affecting the window temperature. The divided inlet schemes can effectively reduce the maximum temperature on the window. The maximum temperature change on the window in the non-uniform inlet velocity is complicated. The proposed target can get same temperature with small mass flow rate. The velocity near the window is the main influence of the window temperature. And the maximum temperature on the window reduces with a rise in the velocity near the window surface. Further, the methods to increase the velocity on the window are being investigated by numerical simulation.

Acknowledgements

This work was supported by "Strategic Priority Research Program" of Chinese Academy of Sciences (Grant No. XDA03040000) and the National Natural Science Foundation of China (Grant No. 51408585). The authors gratefully acknowledge the support of other FDS team members.

Reference

Abderrahim, H., Baeten, P., Bruyn, D.D., et al., 2012. MYRRHA – a multi- purpose fast spectrum research reactor. Energy Convers. Manage. 63, 4–10.
Alamo, A., 2003. Irradiation effects in martensitic steels under neutron and proton mixed spectrum-SPIRE final scientific and technical report. European Commission.
ANSYS Incorporated, 2011. Cfx 14 Manuals.
Bauer, G.S., 2010. Overview on spallation target design concepts and related materials issues. J. Nucl. Mater. 398, 19–27.
Cho, C., Tak, N., Choi, J., et al., 2008. CFD analysis of the HYPER spallation target. Ann. Nucl. Energy 35, 1256–1263.
Cinotti, L., Gherardi, G., 2002. The Pb-Bi cooled XADS status of development. J. Nucl. Mater. 301, 8–14.
Cinotti, L. et al., 2003. Statues of the Studies performed by European Industry on the LBE cooled XADS. In: Proceedings of the International Workshop on P&T and ADS Development, ISBN9076971072.
Class, A.G., Angeli, D., Batta, A., et al., 2011. XT-ADS Windowless spallation target thermohydraulic design & experimental setup. J. Nucl. Mater. 415, 378–384.
Coors, D., Freudenstein, K., Vanvor, D., 2004. Target units for XADS primary systems. In: Sixth European Commission Conference on the Management and Disposal of Radioactive Waste, Luxembourg, March 29–31.
DOE, 1999. A Roadmap for developing accelerator transmutation of waste (ATW) Technology. DOE/RW-0519.
Huang, Q., Li, Y., Chen, Y., 2014. Study of irradiation effects in China low activation martensitic steel CLAM. J. Nucl. Mater. 329, 268–272.
Kikuchi, K., 2009. ADS development in Japan. In: Workshop on AHIPA, Fermi, Oct. 2009.
Knebel, J.U., Cheng, X., Lefhalm, C.H., et al., 2000. Design and corrosion study of a closed spallation target module of an accelerator-driven system (ADS). Nucl. Eng. Des. 202, 279–296.
Mukaiyama, T., Takizuka, T., Mizumoto, M., et al., 2001. Review of research and development of accelerator-driven system in japan for transmutation of long-lived nuclides. Prog. Nucl. Energy 38, 107–134.
Nifenecker, H., Meplan, O., David, S., 2003. Acceleator driven subcritical reactors. Institute of Physics Publishing, ISBN 0-7503-0743-9.
OECD/NEA, 2005. Accelerator and spallation target technologies for ADS applications. In: OECD Nuclear Energy Agency, ISBN92-64-10156-4.
Park, W., Shin, U., Han, S., et al., 2000. HYPER (Hybrid Power Extraction Reactor): a system for clean nuclear energy. Nucl. Eng. Des. 199, 155–165.
Qiu, L., Wu, Y., Xiao, B., et al., 2000. A low aspect ratio tokamak transmutation system. Nucl. Fusion 40, 629–633.
Saito, S., Tsujimoto, K., Kikuchi, K., et al., 2006. Design optimization of ADS plant proposed by JAERI. Nucl. Instrum. Methods 562, 646–649.
Song, T., Tak, N., 2003. Optimal design of HYPER target system based on the thermal and structure analysis of Pb-Bi spallation target and beam window. Ann. Nucl. Energy 30 (12), 1297–1308.
Tak, N., Neitzel, H., Cheng, X., 2005. Computational fluid dynamics analysis of spallation target for experimental accelerator-driven transmutation system. Nucl. Eng. Des. 235, 761–772.
Tsujimoto, K., Oigawa, H., Ouchi, N., et al., 2007. Research and development program on accelerator driven subcritical system in JAEA. J. Nucl. Sci. Technol. 44 (3), 483–490.
Wu, Y., 2016a. Design and R&D progress of China lead-based reactor for ADS research facility. Engineering 2 (1), 124–131.
Wu, Y., 2016b. CLEAR-S: an integrated non-nuclear test facility for china lead-based research reactor. Int. J. Energy Res. http://dx.doi.org/10.1002/er.3569.
Wu, Y., Jiang, J., Wang, M., et al., 2011. A fusion-driven subcritical system concept based on viable technologies. Nucl. Fusion 51 (10), 103036.1–103036.7.
Wu, Y., Song, J., Zheng, H., et al., 2015. CAD-based Monte Carlo program for integrated simulation of nuclear system SuperMC. Ann. Nucl. Energy 82, 161–168.
Wu, Y., Bai, Y., Song, Y., et al., 2016c. Development strategy and conceptual design of China lead-based research reactor. Ann. Nucl. Energy 87, 511–516.
Zhan, W., Xu, H., 2012. Advanced fission energy program – ADS transmutation system. Bull. Chin. Acad. Sci.